

Joint Scale-Lag Diversity in Mobile Ultra-Wideband Systems

Adam R. Margetts and Philip Schniter

Dept. of Electrical and Computer Engineering, The Ohio State University, Columbus, OH
 {margetta, schniter}@ece.osu.edu

Abstract—In this paper, we consider the effect of mobility on an ultra-wideband (UWB) direct sequence spread spectrum communication system. Based on a uniform ring of scatterers model, we determine that the wideband scattering function has a “bathtub-shaped” scale spectrum. We compare the performances of a *scale-lag* Rake and a *frequency-lag* Rake, each capable of leveraging the diversity that results from mobility. The scale-lag Rake receiver, whose scale- and lag-shifted basis functions are matched to the dilation-delay dynamics of the wideband channel, exploits greater diversity. Finally, we suggest a low-complexity implementation of the scale-lag Rake receiver.

I. INTRODUCTION

Ultra wideband (UWB) communication systems are defined by a ratio of single-sided bandwidth to center frequency in excess of 0.25. We point out that the combined effects of multipath and mobility in UWB systems should be modeled differently than in narrowband systems. For example, in UWB systems with a dense ring of scatterers surrounding the receiver, mobility imparts a spreading of the *time-support* of the signal, called *scale spreading*.¹ By scale spreading, we mean that several copies of the transmitted signal combine at the receiver, each with a different dilation of the time support of the original signal. In addition, each copy may be temporally delayed by a different amount. For UWB direct-sequence spread spectrum (DSSS) signaling, we study a *scale-lag Rake receiver* that exploits this diversity.²

The organization of the paper is as follows: Section II introduces the wideband system model, and in Section III, we derive the wideband scattering function for a uniform ring of scatterers and see that the scale-spreading induces a “bathtub-shaped” scale spectrum. In Section IV, we compare the performance of the scale-lag Rake with a frequency-lag Rake [2] and show that the scale-lag Rake exploits greater diversity from the wideband channel. Finally, we propose a low complexity implementation of the scale-lag Rake receiver.

The analysis can be applied to underwater acoustic systems [3] as well as to radio frequency UWB systems [4].

This work was supported in part by the Ohio Space Grant Consortium.

¹Note that scale-spreading is actually a general concept that applies to both narrowband and UWB systems. For example, changing the time scale of a sinusoidal signal is equivalent to shifting the signal in frequency.

²The possibility of a scale-lag receiver was mentioned in [1], but no details were developed.

II. SYSTEM MODEL

A. Transmit Signal

The wideband DSSS waveform is

$$x(t) = \frac{1}{\sqrt{N_p}} \sum_{i=0}^{N_p-1} c_i p(t - iT_o), \quad (1)$$

where $\{c_i\}$ is the length- N_p PN chip sequence, $p(t)$ is the unit-energy chip waveform, and T_o is the chip duration. The symbol duration is $T_s = N_p T_o$ seconds and the system bandwidth is defined to be $W = 1/T_o$. A PN sequence chosen from a ternary alphabet $\{-1, 0, 1\}$ may be used to model time-hopping [4] or episodic signaling [5] without affecting the analysis. In this paper, we consider only baseband signaling; thus, all signals and parameters are real valued. We linearly modulate the DSSS waveform $x(t)$ with a sequence of N_b symbols $\{b_j\}$ to obtain the transmitted signal.

B. Wideband Channel Kernel

Analogous to the spreading function in narrowband signaling, the wideband signal input-output relationship can be modeled by the linear transformation $y(t) = \mathcal{L}\{x(t)\}$ [1] defined by:

$$y(t) = \iint \mathcal{L}(a, \tau) \frac{1}{\sqrt{a}} x\left(\frac{t-\tau}{a}\right) da d\tau, \quad (2)$$

where $x(t)$ is the channel input and $\mathcal{L}(a, \tau)$ is the *wideband channel kernel*. Note that the wideband channel transformation is *not* shift-invariant; hence, sinusoids are *not* eigenfunctions. The wideband channel kernel $\mathcal{L}(a, \tau)$ quantifies the scale-lag spreading produced by the channel—the variable a corresponds to the dilation introduced by the channel, and the variable τ corresponds to the propagation delay.

C. Received Signal

We assume the symbol duration T_s is much larger than the delay spread τ_{max} ; hence, we can ignore inter-symbol interference (ISI) and without loss of generality assume one-shot transmission. Let $x(t)$ be linearly modulated by a data symbol b with energy E_b . The received signal $r(t)$ in additive white Gaussian noise $w(t)$ with two-sided power spectral density of $N_o/2$ is

$$r(t) = \mathcal{L}\{bx(t)\} + w(t), \quad (3)$$

$$= by(t) + w(t). \quad (4)$$

where $y(t)$ is defined in (5).

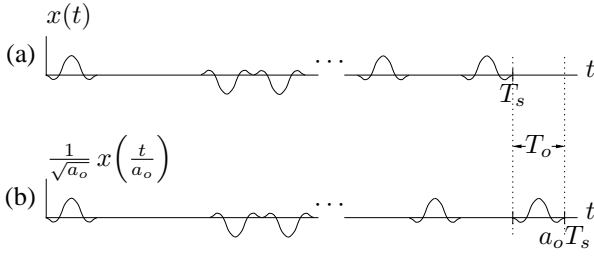


Fig. 1. (a) Transmitted wideband signal. (b) Signal dilated by a_o .

D. Wideband Scale-Lag Canonical Model Representation

Balan et al. [1], inspired by the narrowband frequency-lag canonical model of [2], derived a powerful time-scale canonical model for the wideband transformation (2). The output is simply written as a weighted sum of delayed and dilated versions of the input:

$$y(t) = \sum_{m,n} c_{m,n} \frac{1}{a_o^{m/2}} x\left(\frac{t - nT_o a_o^m}{a_o^m}\right), \quad (5)$$

where the canonical coefficients $c_{m,n}$ are given by,

$$c_{m,n} = \int_0^{\tau_{max}} \int_{a_{min}}^{a_{max}} \mathcal{L}(a, \tau) \text{sinc}\left(n - \frac{\tau}{aT_o}\right) \text{sinc}\left(\frac{\ln(a)}{\ln(a_o)} - m\right) da d\tau. \quad (6)$$

This canonical representation (5) motivates the study of a two-dimensional *scale-lag* Rake receiver.

E. Definitions

In a practice, the wideband channel kernel $\mathcal{L}(a, \tau)$ has finite support: $\{(a, \tau) : a_{min} < a < a_{max}, 0 < \tau < \tau_{max}\}$, where a_{min} and a_{max} are the minimum and maximum dilation, respectively, and τ_{max} is the delay spread. By convention, the time delay of the shortest path is zero lag.

If we consider a system composed of a mobile receiver, fixed reflectors, and a fixed transmitter, the minimum dilation and maximum dilation are $a_{min} = 1 - v_{max}/c$ and $a_{max} = 1 + v_{max}/c$, respectively, where v_{max} is the maximum mobile velocity. However, we note that the wideband kernel can be used to model any dynamic geometry between the transmitter, scatters, and receiver, e.g., a turbulent underwater environment with rings of scatters moving at different speeds.

An important system parameter is the wideband *scale spread*: $\gamma_{max} := \frac{a_{max} - a_{min}}{2} = v_{max}/c = a_{max} - 1$, which defines the maximum deviation from unit temporal dilation.

Consider the inner product of $x(t)$ with $x(t)$ dilated by a :

$$\left\langle x(t), \frac{1}{\sqrt{a}} x\left(\frac{t}{a}\right) \right\rangle. \quad (7)$$

Let $a = a_o$ result in a dilation by one chip period, (illustrated by Fig. 1) or in other words, let a_o satisfy the relation

$$a_o T_s - T_s = T_o \Leftrightarrow a_o = 1 + 1/N_p. \quad (8)$$

The expected value of the inner product (7) evaluated at $a = a_o$ vanishes if and only if the pulse-shape has zero

DC component [6]. Hence, we define a_o as the *minimum resolvable dilation*. Equivalently, $\gamma_o := a_o - 1$ is the *scale resolution* of the wideband DSSS signal $x(t)$. We have $\gamma_o = T_o/T_s = 1/T_s W = 1/N_p$, i.e., the scale resolution is the inverse of the time-bandwidth product.

A useful quantity is the *normalized scale spread*: $\frac{\gamma_{max}}{\gamma_o}$ which can be written in terms of the velocity, speed of signal propagation, and the time-bandwidth product: $\frac{\gamma_{max}}{\gamma_o} = \frac{v_{max}}{c} T_s W$. Note the similarity to the narrowband normalized Doppler-frequency spread [7]: $f_d T_s = \frac{v_{max}}{c} T_s f_c$, where f_c is the carrier frequency.

III. SCATTERING FUNCTION

In the following, we compute the wideband scattering function assuming the wideband channel kernel can be modeled as a sum of N discrete paths:

$$\mathcal{L}(a, \tau) = \sum_{n=0}^{N-1} \ell_n \delta(a - a_n) \delta(\tau - \tau_n), \quad (9)$$

where the n^{th} path has real-valued gain ℓ_n , dilation a_n , and lag τ_n . A similar assumption is used to derive the channel autocorrelation function in the narrowband setting [8].

In order to proceed with the derivation, we make the following assumptions on the statistics of the wideband kernel:

- (A1) The paths are i.i.d., i.e., they have the same joint density between the gain ℓ_n , dilation a_n , and lag τ_n .
- (A2) The paths have zero mean.
- (A3) The dilation a_n is independent of the amplitude ℓ_n and lag τ_n .
- (A4) The amplitude ℓ_n is correlated with the lag τ_n .

Assumption (A4) is often the case in wireless communications channels where propagation losses manifest as an exponentially decaying function of increasing lag [9].

From assumptions (A1) and (A2) we write

$$\begin{aligned} \mathbb{E}[\mathcal{L}(a', \tau') \mathcal{L}(a'', \tau'')] &= \mathbb{E}[\delta(a' - a) \delta(a'' - a) \\ &\quad N |\ell|^2 \delta(\tau' - \tau) \delta(\tau'' - \tau)] \quad (10) \end{aligned}$$

For convenience, we have dropped the subscript n . From assumption (A3), we break the expectation in (10) into two parts: an expectation over dilation a , and an expectation over the joint distribution of the gain ℓ and lag τ .

First, the expectation over dilation is,

$$\begin{aligned} \mathbb{E}[\delta(a' - a) \delta(a'' - a)] &= \\ &= \int \delta(a' - a) \delta(a'' - a) p_a(a) da, \\ &= p_a(a') \delta(a' - a''), \quad (11) \end{aligned}$$

where $p_a(a)$ is the probability distribution of the dilation variable a .

Second, the expectation over the joint distribution between gain and lag is,

$$\begin{aligned} \mathbb{E}[N |\ell|^2 \delta(\tau' - \tau) \delta(\tau'' - \tau)] &= \\ &= N \int \int |\ell|^2 \delta(\tau' - \tau) \delta(\tau'' - \tau) \\ &\quad p_{\ell, \tau}(\ell, \tau) d\tau d\ell \\ &= f(\tau') \delta(\tau' - \tau'') \quad (12) \end{aligned}$$

where we define

$$f(\tau) := N p_\tau(\tau) \int |\ell|^2 p_{\ell|\tau}(\ell|\tau) d\ell. \quad (13)$$

The function $f(\tau)$ is essentially the average received energy density as a function of lag τ . Thus, a decaying energy profile can be modeled.

We substitute the expectation outcomes (11) and (12) into (10) to obtain

$$E[\mathcal{L}(a, \tau) \mathcal{L}(a', \tau')] = \underbrace{p_a(a) f(\tau)}_{:=\Psi(a, \tau)} \delta(a - a') \delta(\tau - \tau') \quad (14)$$

where $\Psi(a, \tau)$ is the *scattering function*.

Now that the form of the scattering function has been determined, we investigate the density function of the dilation $p_a(a)$. An often studied channel geometry for the narrowband channel is a fixed transmitter and dense ring of scatterers surrounding the mobile receiver. In this case, the relation between the angle-of-arrival relative to the direction of travel θ and dilation a is

$$a = 1 - \gamma_{max} \cos(\theta). \quad (15)$$

where $\gamma_{max} = \frac{v_{max}}{c}$ is the scale-spread. Given the angle of arrival distribution $p_\theta(\theta)$, it is a simple matter to compute the dilation distribution $p_a(a)$,

$$p_a(a) = \frac{1}{\gamma_{max}} p_Y \left(-\frac{a-1}{\gamma_{max}} \right), \quad (16)$$

where $Y = \cos(\theta)$ and

$$p_Y(y) = \frac{p_\theta(\cos^{-1}(y)) + p_\theta(-\cos^{-1}(y))}{\sqrt{1-y^2}}. \quad (17)$$

If the angle of arrival θ is distributed uniformly on $(-\pi, \pi]$, then we have

$$p_Y(y) = \frac{1}{\pi \sqrt{1-y^2}}, \quad |y| < 1, \quad (18)$$

which is a familiar ‘‘bathtub shape’’ [10]. We call the function $p_a(a)|_{a=\gamma+1}$ the *scale spectrum*.

IV. TWO-DIMENSIONAL RAKE RECEIVER

The term ‘‘two-dimensional Rake’’ refers to projecting the received signal onto a basis of frequency-lag or scale-lag shifted waveforms. The definition will become clear when we define the scale-lag and frequency-lag Rake receivers. The motivation for applying a two-dimensional Rake is to exploit a mechanism of diversity in addition to lag³ diversity.

The two-dimensional Rake can be divided into two parts: first, the projection of the received signal onto a basis, and second, the combining of the projection coefficients to form the bit estimate. In the following, we clarify these two parts and state the average bit error rate (BER) expression for a coherent maximal-ratio combining receiver.

³Lag diversity is sometimes called multipath diversity and arises when the receiver is able to resolve signals arriving at different delays.

We project the received signal $r(t)$ onto basis $\{x_{m,n}(t)\}$:

$$r_{m,n} = \langle x_{m,n}(t), r(t) \rangle, \quad (19)$$

$$= b y_{m,n} + w_{m,n}, \quad (20)$$

where $y_{m,n} = \langle x_{m,n}(t), y(t) \rangle$ are the signal coefficients and $w_{m,n} = \langle x_{m,n}(t), w(t) \rangle$ are the noise coefficients.

Next, the coefficients $\{r_{m,n}\}$, $-M \leq m \leq M$ and $0 \leq n \leq N$, are stacked into a vector $\mathbf{r} = \mathbf{b}\mathbf{y} + \mathbf{w}$ and linearly combined to form the bit estimate \hat{b}

$$\hat{b} = \mathbf{c}^T \mathbf{r} \quad (21)$$

$$= \mathbf{b}\mathbf{c}^T \mathbf{y} + \mathbf{c}^T \mathbf{w} \quad (22)$$

where \mathbf{c} is the combining vector. The values M and N are chosen so that a significant portion of the energy is contained in the coefficients. Several possible criteria exist for choosing \mathbf{c} , e.g., maximal-ratio combining, equal-gain combining, or selection combining. In this paper, we assume the projection coefficients \mathbf{y} are perfectly known to the receiver, and maximal-ratio combining $\mathbf{c} = \mathbf{y}$ is used to minimize BER.

The BER expression, given the coefficients fade according to a real-valued Gaussian distribution, i.e., $\mathbf{y} \sim \mathcal{N}(\mathbf{0}, \mathbf{\Sigma})$, is [11]

$$P_e = \frac{1}{\pi} \int_0^{\pi/2} \prod_{i=0}^{\kappa-1} \left(\frac{2E_b \lambda_i}{N_o \sin^2 \theta} + 1 \right)^{-1/2} d\theta, \quad (23)$$

$$\leq \frac{1}{2} \prod_{i=0}^{\kappa-1} \left(\frac{2E_b \lambda_i}{N_o} + 1 \right)^{-1/2}. \quad (24)$$

where $\kappa = (2M+1)(N+1)$, and $\{\lambda_i\}$ are the eigenvalues of the correlation matrix $E[\mathbf{y}\mathbf{y}^T] = \mathbf{\Sigma}$.

A. Scale-Lag Rake Receiver

Motivated by (5), and to match the scale-lag spreading of the wideband channel, it is natural to choose as basis functions the set of dilated-delayed versions of the DSSS transmitted signal:

$$x_{m,n}(t) = \frac{1}{a_o^{m/2}} x \left(\frac{t - n a_o^m T_o}{a_o^m} \right), \quad (25)$$

where a_o is the minimum resolvable dilation and T_o is the chip duration. Together, the scale-lag resolution properties (defined in Section II-E) of the basis signals imply that $\langle x_{m,n}(t), x_{\bar{m},\bar{n}}(t) \rangle \approx \delta_{m-\bar{m}} \delta_{n-\bar{n}}$, where δ_n is the Kronecker delta function. Hence, the noise coefficients are approximately uncorrelated. In [6], we showed that the scale-lag Rake receiver outperforms the conventional lag-only Rake receiver, which ignores dilation components in the channel.

The coefficients $\{r_{m,n}\}$ are effectively a sampling of the scale-lag plane, as shown in Fig. 2. A Taylor's series approximation around $a_o = 1$ gives $a_o^m \approx 1 + m(a_o - 1) = 1 + m\gamma_o$; hence, a uniform spacing in the scale domain suffices for typical values of dilation (i.e., $a \approx 1$).

For the unit-energy second-derivative Gaussian pulse [12],⁴

$$p(t) = \frac{\sqrt{f_o} \sqrt[4]{32\pi}}{\sqrt{3}} [1 - 2(\pi f_o (t - T_o/2))^2] \exp(-(\pi f_o (t - T_o/2))^2), \quad (26)$$

⁴We wish to point out that other zero-DC component signals may be used, such as the modified duobinary pulse [7].

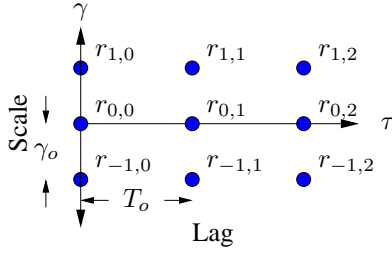


Fig. 2. Sampling the scale-lag plane.

it can be shown⁵ that for large N_p , the correlations can be approximated by

$$\begin{aligned} E[y_{m,n}y_{\bar{m},\bar{n}}] &\approx \int_0^{\frac{\tau_{max}}{T_o}} \int_{-\frac{\gamma_{max}}{\gamma_o}}^{\frac{\gamma_{max}}{\gamma_o}} \Psi(1 - \gamma_o\delta, \tilde{\tau}T_o) \\ &\quad \bar{\chi}(m + \delta, n - \tilde{\tau})\bar{\chi}(\bar{m} + \delta, \bar{n} - \tilde{\tau})d\delta d\tilde{\tau}, \quad (27) \end{aligned}$$

where, for $f_o = 2/T_o$, we have

$$\begin{aligned} \bar{\chi}(\delta, \tilde{\tau}) &= \frac{1}{12} \sum_{k=0}^4 w_k \int_0^1 x^k e^{-2\pi^2(\delta x + \tilde{\tau})^2} dx, \quad (28) \\ w_0 &= 12 - 96\pi^2\tilde{\tau}^2 + 64\pi^4\tilde{\tau}^4, \\ w_1 &= 256\pi^4\tilde{\tau}^3\delta - 192\pi^2\tilde{\tau}\delta, \\ w_2 &= 24(16\pi^4\tilde{\tau}^2\delta^2 - 4\pi^2\delta^2), \\ w_3 &= 256\pi^4\tilde{\tau}\delta^3, \\ w_4 &= 64\pi^4\delta^4. \end{aligned}$$

B. Frequency-lag Rake Receiver

The frequency-lag basis functions are uniform frequency- and time-shifted versions of the DSSS waveform:

$$\tilde{x}_{m,n}(t) := \begin{cases} \sqrt{2} \cos\left(\frac{2\pi mt}{T_s}\right) x(t - nT_o) & m \neq 0 \\ x(t - nT_o) & m = 0 \end{cases} \quad (29)$$

In [2], it is shown that the complex-valued extension of the frequency-lag basis (29) is approximately orthonormal, which motivated using the frequency-lag Rake receiver to exploit diversity in doubly-spread narrowband channels.

For the frequency-lag basis (29) employing unit energy second-derivative pulses (26), it can be shown⁵ that for large N_p , the autocorrelation can be approximated by

$$\begin{aligned} E[y_{m,n}y_{\bar{m},\bar{n}}] &\approx \int_0^{\frac{\tau_{max}}{T_o}} \int_{-\frac{\gamma_{max}}{\gamma_o}}^{\frac{\gamma_{max}}{\gamma_o}} \Psi(1 - \gamma_o\delta, \tilde{\tau}T_o) \\ &\quad \bar{R}_{m,n}(\delta, \tilde{\tau})\bar{R}_{\bar{m},\bar{n}}(\delta, \tilde{\tau})d\delta d\tilde{\tau}, \quad (30) \end{aligned}$$

where

$$\bar{R}_{m,n}(\delta, \tilde{\tau}) = \int_0^1 \sqrt{2} \cos(2\pi mx) R_p((\delta x - n + \tilde{\tau})T_o) dx \quad (31)$$

and $R_p(\tau)$ is the autocorrelation

$$\begin{aligned} R_p(\tau) &= \int p(t)p(t - \tau)dt, \\ &= \frac{1}{3} \left((\pi f_o\tau)^4 - 6(\pi f_o\tau)^2 + 3 \right) \exp\left(-\frac{(\pi f_o\tau)^2}{2}\right). \end{aligned}$$

⁵Contact the authors for derivation details.

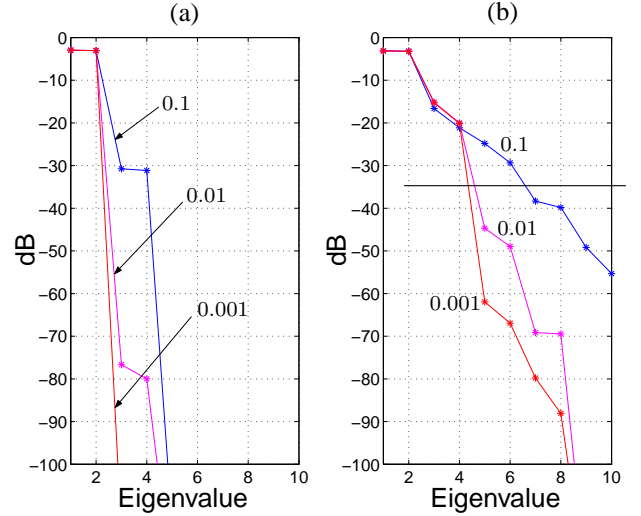


Fig. 3. Eigenvalues of (a) frequency-lag Rake, (b) scale-lag Rake. The curves are indexed by the normalized scale spread $\frac{\gamma_{max}}{\gamma_o} = 0.1, 0.01, \text{ and } 0.001$. The normalized delay spread is $\frac{\tau_{max}}{T_o} = 1$. A “bathtub-shaped” scale spectrum (18) is assumed.

C. Performance Comparison

In this section, we compare the diversity exploited by the scale-lag basis with the diversity exploited by the real-valued frequency-lag basis (similar to the complex-valued basis in [2]). The scale-lag basis is expected to exploit greater diversity in wideband channels since it is more closely matched to the channel dynamics.

Eigenvalue profiles of the scale-lag and frequency-lag Rake receivers are shown in Fig. 3, given that the chip pulse shape $p(t)$ is a second-derivative Gaussian pulse (26). The normalized delay spread is $\tau_{max}/T_o = 1$ chip, and the power profile $f(\tau)$ is assumed to be constant; furthermore, we assume a uniform ring of scatterers and use the “bathtub” scale spectrum specified in Section III. The number of basis functions for each basis is set by $M = \left\lfloor \frac{\gamma_{max}}{\gamma_o} \right\rfloor + 1$ and $N = \left\lfloor \frac{\tau_{max}}{T_o} \right\rfloor + 1$ in order to capture a significant portion of the received energy.

The normalized scale spread of $\frac{\gamma_{max}}{\gamma_o} = \frac{v_{max}}{c} WT_s = 0.001$ would be common in practical RF systems; for example, in an RF system with mobile velocity of 10 km/hr, data rate of 10 kbps, and bandwidth of 1 GHz, or likewise in an RF system with velocity of 100 km/hr, data rate of 1 Mbps, and bandwidth of 10 GHz. A normalized scale spread of 0.1 would occur in a practical underwater acoustic telemetry system with mobile velocity of 15 km/hr, data rate of 1000 bps, and bandwidth of 36 kHz.

It is easy to see by comparing the third and fourth eigenvalues of the profile that the scale-lag Rake will outperform the frequency-lag Rake. This is verified by Fig. 4, which shows the BER performances of the two receivers. Note the large diversity advantage of the scale-lag Rake receiver, whose basis functions are more closely matched to the dilation-delay dynamics of the wideband channel.

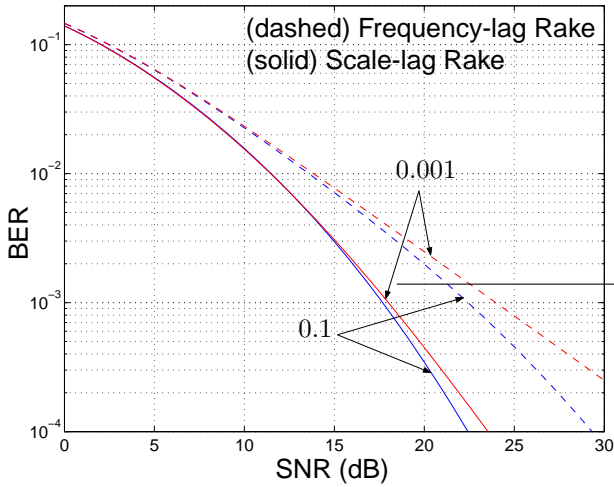


Fig. 4. Same system setup as Fig. 3.

D. Scale-Lag Projection Implementation

In this section, we construct a low-complexity scale-lag projection implementation centered on feeding the output of the chip matched filter into a bank of samplers with frequencies $1/a_o^m T_o$, $m \in \{-M, \dots, M\}$. This can be seen by writing the projection in the following form:

$$\begin{aligned}
 r_{m,n} &= \int x_{m,n}(t)r(t)dt, \\
 &= \int \frac{1}{a_o^{m/2}}x\left(\frac{t-nT_o a_o^m}{a_o^m}\right)r(t)dt, \\
 &= \frac{1}{a_o^{m/2}}\sum_{i=0}^{N_p-1}\frac{c_i}{N_p}\int p\left(\frac{t-nT_o a_o^m-iT_o a_o^m}{a_o^m}\right)r(t)dt, \\
 &= \frac{1}{a_o^{m/2}}\sum_{i=0}^{N_p-1}\frac{c_i}{N_p}p\left(-\frac{t}{a_o^m}\right)*r(t)\Bigg|_{t=(n+i)a_o^m T_o}, \\
 &\approx \frac{1}{a_o^{m/2}}\sum_{i=0}^{N_p-1}\frac{c_i}{N_p}p(-t)*r(t)\Bigg|_{t=(n+i)a_o^m T_o}, \\
 &= \frac{1}{a_o^{m/2}}\sum_{i=0}^{N_p-1}\frac{c_i}{N_p}z_{m,n}[i], \tag{32}
 \end{aligned}$$

where $*$ denotes linear convolution and

$$z_{m,n}[i] = p(-t)*r(t)\Bigg|_{t=(n+i)a_o^m T_o}. \tag{33}$$

The approximation in the second to last step of (32) is close because dilating the pulse shape $p(t)$ by a_o^m is insignificant compared to dilating the entire DSSS waveform $x(t)$. A block diagram of the basis projection is shown in Fig. 5.

V. CONCLUSION

We have studied the effect of mobility (i.e., temporal variation in the physical geometries between transmitter, receiver, and scatterers) on UWB systems and designed receivers capable of leveraging the potential diversity gains that result from multipath propagation in mobile environments.

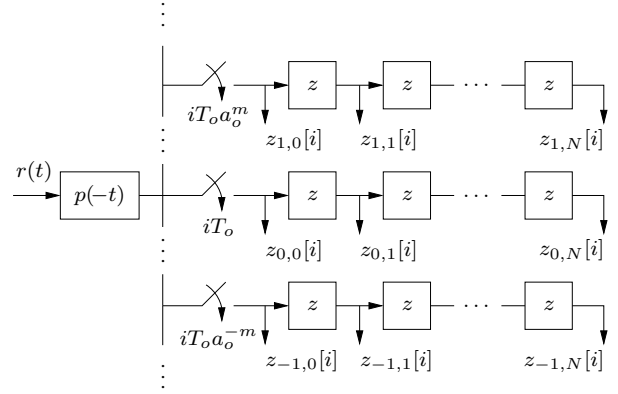


Fig. 5. Scale-lag Rake receiver implementation.

We derived the wideband scattering function for a uniform ring of scatterers and found that the scale-spreading induces a “bathtub-shaped” scale spectrum. We compared the performance of the scale-lag Rake with a frequency-lag Rake [2] and showed that the scale-lag Rake exploits greater diversity since its dilated-delayed basis waveforms are better matched to the wideband channel scale-lag spreading. Finally, we proposed a low complexity implementation of the scale-lag Rake receiver based on applying a bank of samplers to the output of the pulse matched filter.

Future work will concentrate on characterizing the time variations of the scale-lag projection coefficients and developing estimation and tracking schemes.

REFERENCES

- [1] R. Balan, H. V. Poor, S. Rickard, and S. Verdú, “Time-frequency and time-scale canonical representations of doubly spread channels,” *Proc. European Signal Processing Conf.*, Sep. 2004.
- [2] A. M. Sayeed and B. Aazhang, “Joint multipath-doppler diversity in mobile wireless communications,” *IEEE Trans. on Communications*, vol. 47, pp. 123–132, Jan. 1999.
- [3] J. Davies, S. Pointer, and S. Dunn, “Wideband acoustic communications dispelling narrowband myths,” *OCEANS 2000 MTS/IEEE Conference and Exhibition*, vol. 1, pp. 377–384, Sep. 2000.
- [4] M. Win and R. Scholtz, “Ultra-wide bandwidth time-hopping spread-spectrum impulse radio for wireless multiple-access communications,” *IEEE Trans. on Communications*, vol. 48, pp. 679–689, Apr. 2000.
- [5] B. M. Sadler and A. Swami, “On the performance of episodic UWB and direct-sequence communication systems,” *IEEE Trans. on Wireless Communications*, 2004. accepted for publication.
- [6] A. R. Margetts, P. Schniter, and A. Swami, “Scale-lag diversity reception in mobile wideband channels,” *Proc. IEEE Internat. Conf. on Acoustics, Speech, and Signal Processing*, May 2005.
- [7] J. Proakis, *Digital Communications*. New York, NY: McGraw-Hill, 3rd ed., 1995.
- [8] G. L. Stuber, *Principles of Mobile Communications*. Kluwer Academic, 1996.
- [9] M. Terri, A. Hong, G. Guibe, and F. Legrand, “Major characteristics of UWB indoor transmission for simulation,” *Proc. IEEE Vehicular Technology Conference*, vol. 1, pp. 19–23, Apr. 2003.
- [10] W. Jakes, *Microwave Mobile Communications*. Piscataway, NJ: IEEE press, 1993.
- [11] M. K. Simon and M.-S. Alouini, “A unified approach to the performance analysis of digital communication over generalized fading channels,” *Proceedings of the IEEE*, vol. 86, pp. 1860–1877, Sept. 1998.
- [12] A. Swami, B. Sadler, and J. Turner, “On the coexistence of ultra-wideband and narrowband radio systems,” *Military Communications Conference*, vol. 1, pp. 16–19, Oct. 2001.